

Antibacterial activity of silver nanoparticles against *Xanthomonas compestris* var. *compestris*

Meng Li, Tianya Lei, Jiaxuan Li, Xinyu Li, Zhenlin Wei*

College of Life Sciences, Dezhou University, Shandong 253023 China

*Corresponding author, e-mail: wzl19741028@163.com

Received 14 Apr 2024, Accepted 7 Nov 2024

Available online 17 Mar 2025

ABSTRACT: Cabbage black rot, a disease caused by *Xanthomonas compestris* var. *compestris* (Xcc), has significantly impeded the growth and development of Chinese cabbage. In this research, silver nanoparticles (AgNPs) were synthesized using *Solidago canadensis* as the primary material, and their capacity to inhibit the growth of black rot pathogens was evaluated. The results indicated that the AgNPs exhibited a spherical morphology with an average particle size of 10.22 nm. The minimum inhibitory concentration (MIC) and the minimum bactericidal concentration (MBC) against Xcc were determined to be 10 µg/ml. In particular, the inhibition circle assay and growth curve evaluation showed a profound suppressive effect of AgNPs on bacterial proliferation. Furthermore, treatment with AgNPs resulted in structural damage to bacterial cells, a reduction in hydrogen peroxide tolerance, and significantly hindered biofilm development. Synergistic evaluations with Zhongshengmycin, an aminoglycoside antibiotic, highlighted a significant collaborative effect in enhancing resistance to black rot with a Fractional Inhibitory Concentration (FIC) index of 0.335. These *in vitro* results showed that the combined application of 1.25 µg/ml AgNPs and 0.25 µg/ml Zhongshengmycin could inhibit pathogen infestation on explants and thus significantly reduce the dose of antibiotics in production. This study can potentially provide novel insights into preventing and treating cabbage black rot.

KEYWORDS: nanosilver, cabbage black rot, antibacterial, *S. canadensis*

INTRODUCTION

Black rot, a significant disease affecting cruciferous vegetables globally, primarily impacts various parts of these plants, resulting in an annual yield loss ranging from 10 to 50% [1]. Xcc, a rod-shaped Gram-negative bacterium measuring $(0.7\text{--}3) \times (0.4\text{--}0.5)$ µm, is the causative agent. The pathogen infiltrates the plant vascular system through hydathodes or wounds inflicted by machinery or insects [2]. Subsequently, the polysaccharide substances produced by the bacterium obstruct the ducts, hindering the water flow within the conduction system. This blockade results in vein darkening, leaf tissue necrosis, and V-shaped chlorotic lesions. The affected tissues may experience necrosis, resulting in premature leaf shedding or even the demise of young plants [2]. Xcc encompasses a wide range affecting numerous species within the *Brassicaceae* family, including economically important vegetable crops within this family such as cabbage, cauliflower, turnip, rapeseed, broccoli, as well as other *Brassicaceae* plants, ornamental plants, and others. Consequently, black rot has been recognized globally as a highly destructive and yield-limiting disease for cruciferous vegetables [3, 4]. Despite significant advancements in molecular breeding efforts to cultivate plants resistant to Xcc infestation, numerous challenges persist, necessitating further research [5]. Hence, the pursuit of novel, efficacious, and safe antimicrobial agents remains crucial in managing black rot [4].

Due to their small size and surface properties,

AgNPs are optimal antibacterial agents. Furthermore, they exhibit a high level of biosafety, which contributes to their remarkable antimicrobial properties and capacity to inhibit the emergence of drug resistance. As a result, AgNPs have become a potent broad-spectrum antimicrobial agent, and their utilization has expanded across various sectors, including agriculture, medicine, and food, to combat antimicrobial resistance [6–9].

The antimicrobial mechanism of AgNPs is intricate and primarily revolves around the release of Ag⁺ ions, which can be influenced by factors such as particle size and shape [10, 11]. Typically, the antimicrobial activity of AgNPs commences through physical interaction with the cell membrane, leading to its deformation. Upon entry into the cell, Ag⁺ ions interact with intracellular organelles and biomolecules, induce oxidative stress, and alter signal transduction pathways. Furthermore, the released Ag⁺ ions, lipopolysaccharides, and membrane proteins from damaged cell membranes disrupt the transmembrane proton motive force (PMF) and impede the ATP biosynthesis. Furthermore, the synergistic interaction between Ag⁺ ions and oxygen molecules generates significant quantities of reactive oxygen species (ROS), thereby exacerbating the damage to cellular structures and biomolecule functions [12]. Additionally, AgNPs exhibit antibacterial effects by inhibiting ribosome function, causing alterations in DNA structure and function, and obstructing bacterial biofilm formation [11, 13].

The utilization of *Solidago canadensis* as a plant resource is extensive, owing to its abundant anti-

crobial compounds, flavonoids, and other beneficial substances suitable for the eco-friendly synthesis of AgNPs [14]. This research involved the green synthesis of AgNPs using *S. canadensis* extracts, followed by an investigation into their inhibitory efficacy and mechanism against black rot in cabbage. The study demonstrated a remarkable synergistic antibacterial effect between AgNPs and Zhongshengmycin, indicating a substantial reduction in the required dosage of both agents. These findings offer novel strategies for the management of black rot in cabbage.

MATERIALS AND METHODS

Experimental materials

Professor Tao Jun of Hainan University generously provided the Xcc strain, while *S. canadensis* was procured from the Guangxi Province market. The reagents utilized in this study were analytical grades obtained from Sigma-Aldrich (Germany) and Tianjin Kemiou Chemical Reagent Co., Ltd. (Tianjin, China). The fresh turnips (*Raphanus sativus* L) were obtained from the local market. Zhongshengmycin (% content) was purchased from Zhongxun Agrochemical Co., Ltd. (Jiangxi, China).

Preparation and characterization of AgNPs

The leaf tissue of *S. canadensis* was vacuum dried for 24 h at 65 °C and then ground into a fine powder. Subsequently, 10 g of the powder was mixed with 100 ml of distilled water. The mixture was subjected to heating for 20 min and then filtered. The filtrate was combined with a 1 mM silver nitrate solution in a 1:9 ratio by volume. The pH was adjusted to 9, and the solution was synthesized with continuous stirring at 37 °C for 2 h, forming a dark brown solution [15]. This synthesized solution underwent centrifugation at 16,320 g, followed by washing with pure water 3 times and lyophilization to yield AgNP powder [13]. The absorption spectra were measured using a UV spectrophotometer (Evolution 220, Thermo Fisher, USA) with a wavelength of 300–600 nm [16]. Furthermore, the morphology of AgNPs was observed using a Scanning Electron Microscope (SEM, Merline compact, Zeiss, Germany) and a High-Resolution Transmission Electron Microscope (HR-TEM, FEI, Talos F200X G2, Thermo Fisher) [17].

Inhibitory ability of AgNPs against Xcc

The bacteria were cultivated for an extended period in a newly prepared Nutrient Broth medium, with OD₆₀₀ reaching 0.5. Subsequently, the bacterial suspension was further diluted to 4×10^7 colony-forming units per milliliter (CFU/ml) for experimental purposes.

MIC and MBC determination

The MIC of AgNPs against Xcc was determined through a gradient dilution method. The concentration range

of AgNPs tested was 0.94–200 µg/ml. Following an incubation period of 48 h at 28 °C, 10 µl of 0.5% triphenyltetrazolium chloride (TTC, Kemiou, Tianjin, China) staining solution was introduced to each well for 30 min to ascertain the MIC value. The samples added with sterilized water instead of AgNP treatment were used as a control. Subsequently, bacterial samples treated with AgNPs at $4 \times$ MIC, $2 \times$ MIC, $1 \times$ MIC, and $1/2 \times$ MIC concentrations were selected and streaked on Nutrient Agar (NA) solid medium for 48 h to determine the MBC values [6].

Plate diffusion assay

The bacteria were cultured on NA medium and subjected to various treatments: AgNO₃ at 1 mM as the positive control, plant extract as the negative control, and 125, 250, and 500 µg/ml AgNPs in Oxford cups. Each cup received 100 µl of the respective solution, and the incubation was carried out at 28 °C. The diameter of the inhibition zone was recorded after 48 h of incubation [6]. We used 1 mM AgNO₃ solution as positive control.

Growth curve experiment

Freshly cultivated bacterial specimens were treated with AgNPs at the concentrations equivalent to $2 \times$ MIC, $1 \times$ MIC, and $1/2 \times$ MIC. Subsequently, the OD₆₀₀ value of each sample was monitored for a duration of 0 to 8 h, and the resulting data was utilized to construct a growth curve [18]. The sample without AgNP treatment was used as controls.

Inhibition mechanism

Inhibition of biofilm formation

AgNPs were introduced into the bacterial solution at the concentrations of 4, 6, and 8 µg/ml, followed by a 48-h incubation period. Subsequently, the bacterial membranes were rinsed with phosphate buffer saline (PBS) and then fixed with methanol. The bacterial biofilms were stained using a 0.1% crystal violet solution for 15 min, followed by dissolving in 33.3% glacial acetic acid. The OD₅₉₀ values were quantified, and the antibacterial efficacy of the AgNPs was evaluated by comparing the results to the control group [19].

H₂O₂ tolerance

Freshly cultivated bacteria were combined with AgNPs in a 1.5 ml centrifuge tube to achieve the concentrations of $1/4 \times$ MIC, $1/2 \times$ MIC, MIC, and $2 \times$ MIC, respectively. The bacterial mixture underwent incubation in a shaker set at 250 rpm and 28 °C for varying durations of 15 min, 30 min, and 1 h. Subsequently, 5 µl samples of the bacterial culture were withdrawn at each time interval and subjected to gradient dilutions for 4 times (each gradient was diluted 10-fold). These diluted samples were then plated on NA medium supplemented with H₂O₂ at the final concentration of 0.1,

0.25, and 0.5 mM and incubated at 28 °C for 48 h to monitor bacterial growth [20]. Bacterial cells without AgNP treatment were used as controls.

SEM observation of Xcc cell structure disruption

The bacterial cells mixed with AgNPs of 2 × MIC were incubated for 0.5 to 2 h at 250 rpm and a temperature of 28 °C. Following this, centrifugation at 2,420 g was performed, followed by a triple washing cycle using PBS (pH 7.0). The cells were then fixed in a 2.5% glutaraldehyde solution for 4 h, followed by ethanol gradient dehydration. Subsequently, anhydrous ethanol was introduced before the SEM analysis [21]. Bacterial cells without AgNP treatment were used as controls.

Inhibition of three bacterial extracellular enzyme activities by AgNPs

We prepared 3 types of plate media containing 0.5% (w/v) carboxymethyl cellulose, 0.1% starch, and 1% skimmed milk powder, respectively. Also, these plates were supplemented with either 2 or 4 g/ml of AgNP. For the experiments, 2 µl of bacterial solution was taken onto the plates and incubated for 24 h. Subsequently, the starch-containing plates were treated with 2 ml of I2/KI solution (0.08 mol/l I2 and 3.2 mol/l KI) for 10 min, followed by a 10-min wash with 70% alcohol, leading to the manifestation of transparent circles indicative of extracellular amylase activity. For assessing extracellular cellulase activity, 2 ml of 0.1% Congo red was applied for 30 min, followed by 2 washes with pure water and decolorization using 20 ml of 1 mol/l NaCl for 20 min. Extracellular protease activity assay did not require the use of staining. The plates lacking AgNP treatment were employed as controls [22].

Synergistic inhibition of AgNPs with Zhongshengmycin

FIC index analysis

The analysis of the FIC index was conducted using the checkerboard method. Zhongshengmycin and AgNP solutions were administered to the bacteria with Zhongshengmycin concentrations ranging from 0.008 to 1 µg/ml and AgNP concentrations ranging from 0.04 to 20 µg/ml. After 48 h of incubation, 10 µl of 0.5% TTC solution was added to each well, enabling the calculation of MIC and FIC index values for AgNPs and Zhongshengmycin [7]. The FIC index was calculated using the formula: FIC index = (MIC of AgNPs in combination with Zhongshengmycin/MIC of AgNPs alone) + (MIC of Zhongshengmycin in combination with AgNPs/MIC of Zhongshengmycin alone).

In vitro experiments on the bacteriostatic effect of AgNPs

After sterilized by 75% alcohol, the white turnips (*Raphanus sativus* L.) were sliced into 5 mm thick

pieces and placed on moist sterile filter paper. Subsequently, upon reaching a bacterial concentration of 4×10^7 CFU, AgNPs and Zhongshengmycin were individually administered onto the surface of the turnip slices in a 100 µl volume. The study was structured into 4 experimental groups: the positive control group (exposed solely to bacterial solution), treated with 10 µg/ml AgNPs, treated with 1 µg/ml Zhongshengmycin, and treated with 1.25 µg/ml AgNPs combined with 0.25 µg/ml Zhongshengmycin. After a 72-h incubation period, bacterial proliferation was observed [22].

Statistical analysis

The one-way ANOVA method was used for statistical analysis to identify significant differences between the means of the samples tested via the Graphpad Prism program (v. 8.3.0). The asterisks from 1 to 4 represent the different levels of significance of differences between the 2 samples, i.e., $p < 0.05$, 0.01, 0.001, and 0.0001. NS denotes non-statistical significance.

RESULTS AND DISCUSSION

Synthesis of AgNPs

The experimental optimization yielded a change in the color of the reaction solution from light yellow to reddish-brown when employing a 1:9 (v/v) ratio of aqueous extract to AgNO₃ solution with a reaction time of 2 h and a pH of 9. Analysis of the UV-vis scanning spectra showed a distinct Surface Plasmon Resonance (SPR) peak of AgNPs at 410.52 nm, which confirmed the successful synthesis of AgNPs (Fig. 1a) [15]. Furthermore, the localization of SPR peak at 410.52 nm indicated a small particle size distribution [23]. The subsequent SEM-EDS analysis revealed that the synthesized AgNPs exhibited a nearly spherical structure with an average diameter of 10.22 nm (Fig. 1c), in line with AgNPs derived from other plant sources [15]. Previous study has suggested that smaller, spherical AgNPs exhibit improved antibacterial properties [24]. Consequently, the synthesized AgNPs were employed in this study to assess their efficacy against Xcc bacteria.

Inhibitory ability of AgNPs against Xcc

MIC and MBC determination

The findings from the MIC and MBC assays of AgNPs against Xcc revealed that the MIC and MBC values were 10 µg/ml (Fig. S1), which indicated a potent inhibitory effect of the synthesized AgNPs on black rot bacteria. To date, limited research has been reported on utilizing nanomaterials to inhibit Xcc bacteria. At a concentration of 1×10^6 CFU of Xcc bacteria, chemically synthesized AgNPs effectively suppressed Xcc bacterial growth in cabbage seeds at the concentrations of 6.25 µg/ml and above, outperforming traditional hot water treatment [25]. In a separate investigation,

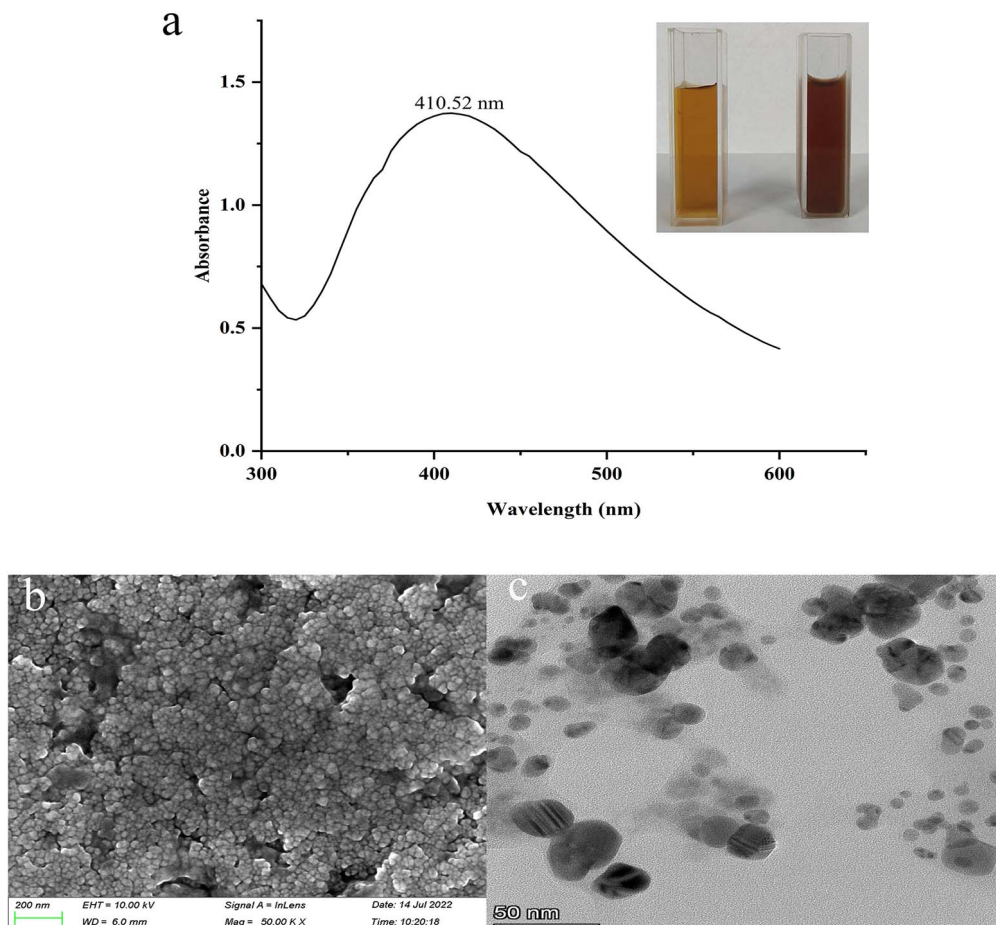


Fig. 1 Characterization of AgNPs. (a) Uv-vis spectra of AgNPs; (b) SEM image of AgNPs; and (c) HR-TEM image of AgNPs.

thymol-loaded chitosan nanoparticles at the concentrations ranging from 100 to 600 $\mu\text{g/ml}$ also exhibited inhibitory effects against Xcc bacteria (at a concentration of 1×10^8 CFU/ml) [26]. Collectively, the AgNPs produced in this study demonstrated superior efficacy against Xcc bacteria.

Plate diffusion experiment against Xcc

This study employed the plate diffusion assay to assess the antibacterial properties of AgNPs against Xcc. The results depicted in Fig. 2 and Fig. S2 demonstrated bacterial growth within the Oxford cups treated with *S. canadensis* aqueous extract, indicating a limited bacterial inhibitory effect of plant extraction possibly attributed to factors like low concentration and absence of treatment. Noteworthy, treatment with 1 mM AgNO_3 displayed the most pronounced inhibition of bacteria, manifesting a circle diameter of 20.55 ± 0.97 mm. The inhibitory efficacy of AgNPs was found to be dose-dependent with diameters for treatments ranging from 125 to 500 $\mu\text{g/ml}$

measuring 12.29 ± 1.06 mm, 13.73 ± 0.24 mm, and 15.10 ± 0.86 mm, respectively (Fig. 2a). While no significant differences were observed in the circle of inhibition diameters between the 125 and 250 $\mu\text{g/ml}$ treatments as well as between the 250 and 500 $\mu\text{g/ml}$ treatments, a significant disparity was noted between the 125 and 500 $\mu\text{g/ml}$ treatment ($p < 0.05$).

We also found significant differences in the results of plate diffusion experiment in the AgNP-treated group compared to the 1 mM AgNO_3 treated group, even though the MIC and MBC values for the AgNPs were both 10 $\mu\text{g/ml}$. Similar results have been found in other studies [27]. In their study, the MIC value of AgNPs against *E. coli* was found to be 12 $\mu\text{g/ml}$, but the diameter of the inhibition zone was about 15 mm.

Growth curve experiment

The growth curve analysis indicated that the synthesized AgNPs exhibit a notable inhibitory influence on the growth of Xcc with the extent of inhibition being correlated with the concentration of AgNPs (Fig. 2b).

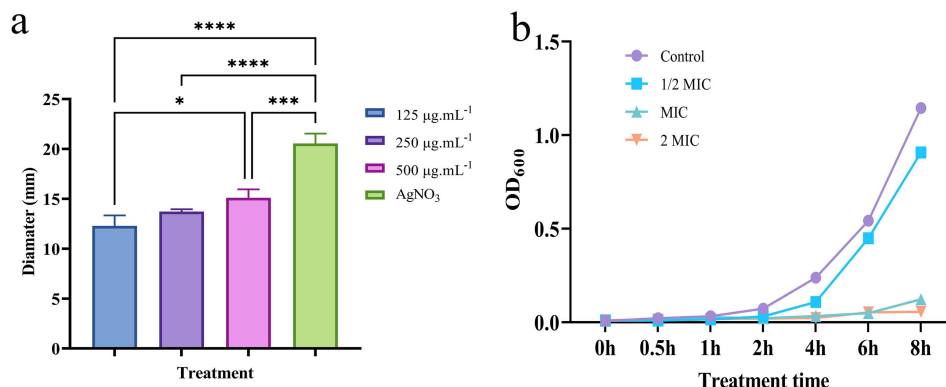


Fig. 2 Plate diffusion and growth curve tests. (a) Plate diffusion test of Xcc treated with AgNO₃ and AgNPs at different concentrations and (b) Growth curve analysis of Xcc treated with AgNPs at different concentrations.

The most potent inhibitory impact was observed at a concentration of 2 × MIC of AgNPs (20 µg/ml), characterized by the bacterial solution’s OD₆₀₀ value remaining below 0.06, thereby impeding bacterial growth significantly. At a concentration of 1 × MIC (10 µg/ml) of AgNPs, bacterial growth was sluggish within the initial 6 h, with the OD₆₀₀ value at 8 h recorded as 0.123 ± 0.058, a result that did not show a significant variance from the treatment with 2 × MIC of AgNPs ($p = 0.414$) but was markedly different from the control group ($p < 0.01$). Conversely, bacterial growth accelerated when treated with AgNPs at 1/2 × MIC concentration (5 µg/ml), recording an OD₆₀₀ value of 0.907 ± 0.032 after 8 h, with no significant difference observed ($p = 0.06$) compared to the OD₆₀₀ value of 1.145 ± 0.079 from the control group, indicating that the 1/2 × MIC AgNP treatment did not exhibit a notable bacteriostatic effect. The outcomes are consistent with the plate diffusion test, which demonstrated the potent inhibitory effects of the AgNPs synthesized in this investigation against Xcc bacteria at 1 × MIC (10 µg/ml).

Mechanisms of AgNPs against Xcc bacteria

Inhibition of biofilm formation

The establishing of a bacterial biofilm creates a proactive environment that promotes the survival and proliferation of bacteria. AgNPs have been identified as the hindrance to the synthesis of biofilms, showcasing an essential bacteriostatic property [19]. Research has indicated that AgNPs, even at concentrations below the MIC [17], can hinder the formation of biofilms. Hence, for this study, AgNP concentrations ranging from 4–8 µg/ml were utilized. The findings in this study revealed a substantial and dose-dependent suppressive impact of AgNPs on Xcc biofilm formation (Fig. 3), as evidenced by the decrease in the OD₅₉₀ value with increasing AgNP concentrations, signifying a higher level of bacterial membrane inhibition. Notably, biofilms

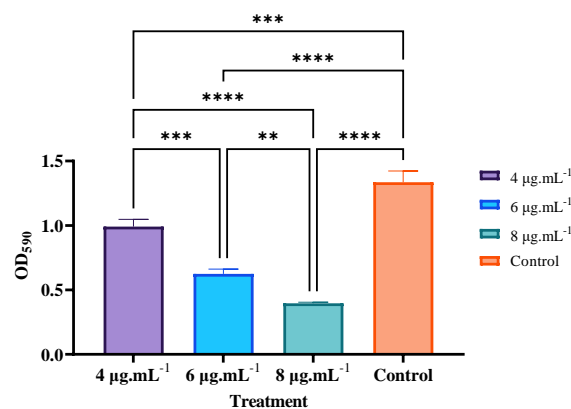


Fig. 3 Inhibition of Xcc biofilm formation by AgNPs.

formed under a 4 µg/ml AgNP concentration exhibited a highly significant variance ($p < 0.0001$) compared to the control group. Furthermore, significant differences were observed between the 4 and 6 µg/ml treatments as well as between the 6 and 8 µg/ml treatments. Consequently, the application of lower concentrations of AgNPs effectively impedes the formation of Xcc biofilms, thereby exerting a substantial inhibitory influence on the proliferation of this bacterium.

Previous research has illustrated that the inhibitory impact of AgNPs on biofilm formation extends beyond a single mechanism. In addition to impeding biofilm formation, AgNPs have been found to reduce the production of extracellular polymeric substances (EPS), disrupt biofilm structure, and interfere with quorum sensing (QS) signaling [17, 28, 29]. Therefore, the additional examination is necessary to thoroughly comprehend the distinct functions of AgNPs in inhibiting bacterial biofilms.

Mishra et al [30] conducted a study to explore the inhibitory effect of AgNPs on the biofilm formation of *Xanthomonas oryzae* pv. *Oryzae* (Xoo). Utilizing

Stenotrophomonas sp. BHU-S7, they synthesized AgNPs and observed a notable inhibitory effect on Xcc biofilm production even at a concentration as low as 5 $\mu\text{g/ml}$ ($p = 0.001$). These findings suggested that AgNPs synthesized through green methods can impede biofilm synthesis of Xcc, highlighting a crucial aspect in its inhibitory mechanism.

H_2O_2 tolerance assay

The investigation employed an H_2O_2 tolerance assay to assess the redox status of bacterial cells following exposure to varying concentrations of AgNPs at various intervals.

The data indicated a marked decrease in H_2O_2 tolerance among Xcc bacteria exposed to varying levels of AgNPs, as depicted in Fig. S3. Notably, the redox state of bacterial cells varied across different time points, with all treated bacteria failing to proliferate on H_2O_2 plates containing 0.5 mM H_2O_2 . Furthermore, the disparity in colony formation on plates with 0.25 mM H_2O_2 was more evident compared to that with 0.1 mM H_2O_2 . Particularly, a significant reduction in colony formation was observed on plates containing 0.25 mM H_2O_2 and 2.5 $\mu\text{g/ml}$ of AgNPs for 15 min compared to the control group. Moreover, minimal colony growth was observed after a 1-h treatment with 20 $\mu\text{g/ml}$ AgNPs, resulting in substantially fewer colonies than the control and other AgNP-treated groups. It is noteworthy that AgNPs triggered the generation of elevated levels of reactive oxygen species (ROS) as a key inhibitory mechanism [12]. While direct observation of ROS content in Xcc cells was not feasible due to instrumental constraints, the H_2O_2 tolerance assay was utilized as a supplementary method to assess changes in ROS levels under AgNP treatments. The study postulated that AgNP exposure disrupted the redox equilibrium of bacteria, fostering ROS production and ultimately compromising cellular tolerance to H_2O_2 .

Results of SEM microscopy observation

The AgNP-influencing mechanism is widely recognized to involve disruption of bacterial cell membranes and bacteriophage structures. SEM investigations on Xcc bacteria subjected to various AgNP treatments revealed that exposure to 10 $\mu\text{g/ml}$ AgNPs induced significant alterations in bacterial cell morphology within 30 to 120 min. Compared to control (Fig. 4a), following a 30-min treatment with AgNPs, some bacteria displayed pronounced constrictions in the midsection that gradually thickened and shortened, while others experienced ruptures that resulted in content leakage (Fig. 4b). Over time, these constrictions in some cells became less apparent or manifested as pores, ultimately resulting in the disintegration of the cellular structure, with only the skeletal remains remaining visible (Fig. 4c,d).

Inhibition of extracellular enzyme activity by AgNPs

The pathogenicity of Xcc is reliant on the secretion of various extracellular enzymes such as cellulases, pectinases, proteases, and amylases [31]. In addition to causing bacterial cell disintegration and death, the suppression of extracellular enzymes restricts Xcc infestation. To prevent interference with the potent inhibitory impact of high concentrations of AgNPs on bacterial growth, Xcc was exposed to 2 and 4 $\mu\text{g/ml}$ of AgNPs, resulting in no significant growth inhibition. Subsequent evaluation of enzyme activities via plate assay revealed that treatment with 2 $\mu\text{g/ml}$ of AgNPs significantly impeded the activities of all 3 extracellular enzymes (Fig. 5). Notably, protease activity exhibited a hyaline circle diameter of 11.820 ± 0.502 mm following 2 $\mu\text{g/ml}$ AgNP treatment, markedly smaller than that of the control at 13.820 ± 1.022 mm ($p < 0.001$). Conversely, the inhibitory effect on amylase and cellulase activities was more pronounced with 4 $\mu\text{g/ml}$ AgNP treatment compared to that of 2 $\mu\text{g/ml}$ AgNP treatment. For instance, the control circle diameter for amylase was 20.680 ± 0.606 mm. In contrast, after treatment with 2 concentrations of AgNPs, the diameters were 13.990 ± 0.090 mm and 19.387 ± 0.221 mm, respectively, with significant differences compared to control ($p < 0.0001$ and $p < 0.05$). These findings demonstrate the significant inhibitory impact of AgNPs on the activities of these crucial extracellular enzymes, underscoring their roles in the anti-Xcc bacterial mechanism.

Synergistic inhibitory effect between AgNPs and Zhongshengmycin on Xcc

Determination of synergistic antibacterial ability

Zhongshengmycin is a kind of aminoglycoside antibiotic developed by the Chinese Academy of Agricultural Sciences in 1996 with the function of interrupting the synthesis of protein peptide bonds of pathogenic microorganisms. Now, this antibiotic is used as a broad-spectrum agro-antibiotic for controlling crop pathogenic microorganisms, including *X. campestris*, *Erwinia carotovora*, and *Phytophthora piricola* [32]. Although Zhongshengmycin is considered safe and effective for hyperthyroidism, 2 factors have hindered its application. One is the discovery that this compound can be toxic to the lungs of mice [33], and the other is the emergence of Zhongshengmycin-resistant bacteria [34]. Therefore, the combined use of this antibiotic with biologically safe antibacterial substances can control the harm of Zhongshengmycin-resistant bacteria and improve biological safety during its use.

The findings revealed that the MIC of Zhongshengmycin against Xcc bacteria was 1 $\mu\text{g/ml}$ when used alone. However, when this compound was combined with AgNPs, a pronounced synergistic antibacterial effect was observed. In this scenario, the MIC value of AgNPs decreased to 1.25 $\mu\text{g/ml}$, and the

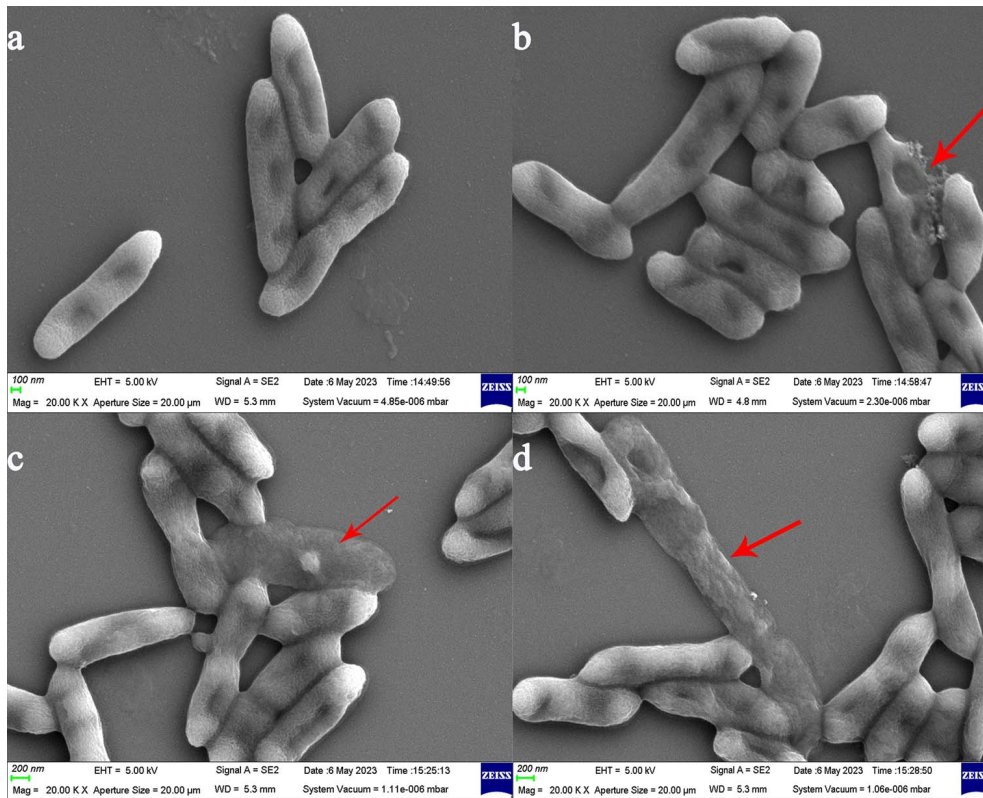


Fig. 4 SEM observation of Xcc under AgNP treatments. (a) Control and (b-d) AgNPs treated for 30, 60, and 120 min, respectively.

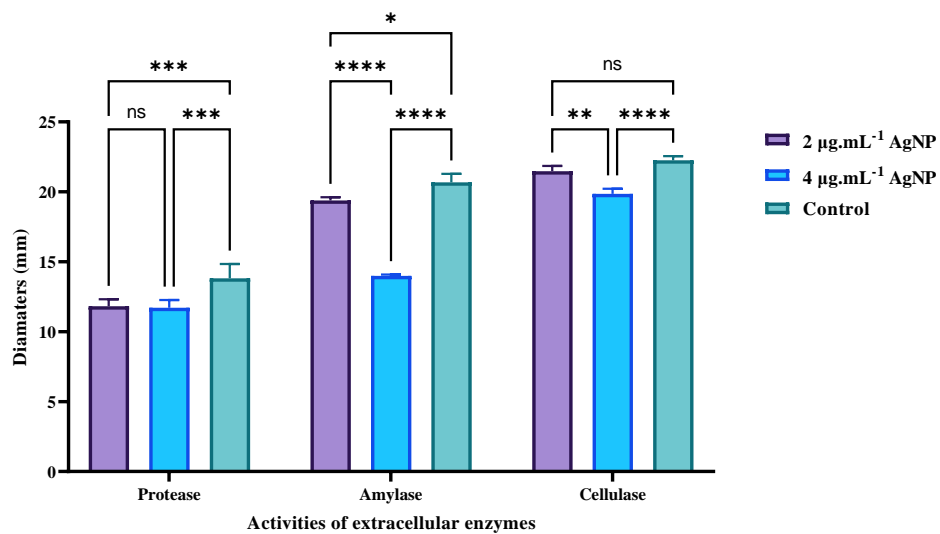


Fig. 5 Inhibition of three extracellular enzyme activities by AgNPs.

MIC value of Zhongshengmycin decreased from 1 to 0.0625 µg/ml (Fig. S4). The FIC is a hierarchical measure of inhibitory concentration that quantifies the combined antimicrobial efficacy of different substances

against a bacterium. An FIC index below 0.5 typically indicates synergism, while values between 0.5 and 1 indicate additivity, values 1 to 2 suggest indifference, and values exceeding 2 denote antagonism. A lower

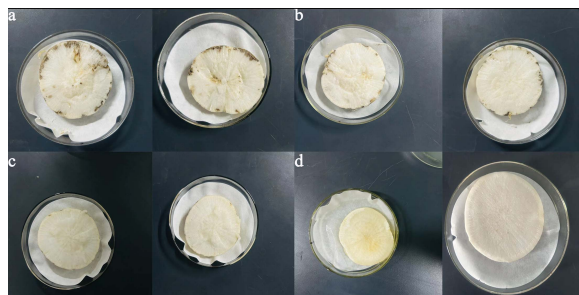


Fig. 6 *In vitro* inhibitory effect of AgNPs in combination with Zhongshengmycin on Xcc. (a) Control explants infected with Xcc; (b) explants treated with Xcc and Zhongshengmycin; (c) explants treated with Xcc and AgNPs; and (d) samples treated with Xcc, AgNPs, and Zhongshengmycin.

FIC index signifies a stronger synergistic relationship between the substances [21]. In the present study, the antimicrobial FIC index of Xcc between AgNPs and Zhongshengmycin was determined to be 0.335, signifying a high level of synergism between the lower concentrations of AgNPs and Zhongshengmycin in inhibiting Xcc. This synergistic combination holds the potential to decrease the utilization of antibiotics in practical applications.

In vitro synergistic inhibition of Xcc by the combination of AgNPs and Zhongshengmycin

Inoculation of radish explants with 4×10^7 CFU of Xcc led to the manifestation of typical black rot symptoms on previously healthy white radish (Fig. 6a). Conversely, the application of 10 $\mu\text{g}/\text{ml}$ AgNPs and 1 $\mu\text{g}/\text{ml}$ Zhongshengmycin effectively suppressed Xcc infestation, resulting in white radish explants free from evident black rot symptoms (Fig. 6b,c), aligning with the outcomes of the MIC test. Co-administration of 1.25 $\mu\text{g}/\text{ml}$ AgNPs+0.25 $\mu\text{g}/\text{ml}$ Zhongshengmycin on Xcc-infected explants yielded white radish devoid of black rot symptoms (Fig. 6d), indicating a notable synergy between the 2 antimicrobial agents, thus potentially reducing the antibiotic dosage required for black rot management.

CONCLUSION

The current investigation involved the synthesis of AgNPs through the reaction between AgNO_3 and the biomaterial *S. canadensis*. The study aimed to evaluate the inhibitory capacity and mechanism of AgNPs against Xcc through a variety of methods, including the zone of inhibition, MIC, MBC, growth curve analysis, biofilm formation inhibition, H_2O_2 tolerance, and SEM observations. The results demonstrated a remarkable antibacterial efficacy of AgNPs against Xcc, as evidenced by inhibition of bacterial growth, disruption of cellular structure, suppression of biofilm formation,

and modulation of extracellular enzyme activities. Furthermore, a significant synergistic effect was observed between AgNPs and Zhongshengmycin, leading to a notable reduction in the consumption of antibiotics. This research presents a novel method for managing black rot disease in cabbage.

Appendix A. Supplementary data

Supplementary data associated with this article can be found at <https://dx.doi.org/10.2306/scienceasia1513-1874.2025.011>.

Acknowledgements: The authors thank Ms. Yang Lu for her technical support.

REFERENCES

- Sharma BB, Kalia P, Singh D, Sharma TR (2017) Introgression of black rot resistance from *Brassica carinata* to Cauliflower (*Brassica oleracea* botrytis group) through embryo rescue. *Front Plant Sci* **8**, 273329.
- Vicente JG, Holub EB (2012) *Xanthomonas campestris* pv. *campestris* (cause of black rot of crucifers) in the genomic era is still a worldwide threat to brassica crops. *Mol Plant Pathol* **14**, 2–18.
- Inoue Y, Fujikawa T, Takikawa Y (2021) Detection and identification of *Xanthomonas campestris* pv. *campestris* and pv. *raphani* by multiplex polymerase chain reaction using specific primers. *Appl Microbiol Biotechnol* **105**, 1991–2002.
- Liu Z, Wang H, Wang J, Lv J, Xie B, Luo S, Wang S, Zhang B, et al (2022) Physical, chemical, and biological control of black rot of brassicaceae vegetables: A review. *Front Microbiol* **13**, 1023826.
- Singh S, Dey SS, Bhatia R, Batley J, Kumar R (2018) Molecular breeding for resistance to black rot [*Xanthomonas campestris* pv. *campestris* (Pammel) Dowson] in Brassicas: recent advances. *Euphytica* **214**, 196.
- Wei Z, Xu S, Jia H, Zhang H (2022) Green synthesis of silver nanoparticles from *Mahonia fortunei* extracts and characterization of its inhibitory effect on Chinese cabbage soft rot pathogen. *Front Microbiol* **13**, 1030261.
- Dove AS, Dzurny DI, Dees WR, Qin N, Nunez Rodriguez CC, Alt LA, Ellward GL, Best JA, et al (2022) Silver nanoparticles enhance the efficacy of aminoglycosides against antibiotic-resistant bacteria. *Front Microbiol* **13**, 1064095.
- Meer SD, Naidoo Y, Dewir YH, Lin J, Rihan HZ (2022) Green synthesis of silver nanoparticles from *Heteropyxis natalensis* leaf extract and their potential antibacterial efficacy. *ScienceAsia* **48**, 196–201.
- Nie P, Zhao Y, Xu H (2023) Synthesis, applications, toxicity and toxicity mechanisms of silver nanoparticles: A review. *Ecotoxicol Environ Saf* **253**, 114636.
- Garg D, Sarkar A, Chand P, Bansal P, Gola D, Sharma S, Khantwal S, Surabhi, et al (2020) Synthesis of silver nanoparticles utilizing various biological systems: mechanisms and applications: A review. *Prog Biomater* **9**, 81–95.
- Huq MA, Ashrafudoulla M, Rahman MM, Balusamy SR, Akter S (2022) Green synthesis and potential antibacterial applications of bioactive silver nanoparticles: A review. *Polymers (Basel)* **14**, 742.

12. Mikhailova EO (2020) Silver nanoparticles: mechanism of action and probable bio-application. *J Funct Biomater* **11**, 84.
13. Kaiser KG, Delattre V, Frost VJ, Buck GW, Phu JV, Fernandez TG, Pavel IE (2023) Nanosilver: an old antibacterial agent with great promise in the fight against antibiotic resistance. *Antibiotics (Basel)* **12**, 1264.
14. Kolodziej B, Kowalski R, Kędzia B (2007) Antibacterial and antimutagenic activity of extracts aboveground parts of three *Solidago* species: *Solidago virgaurea* L., *Solidago canadensis* L. and *Solidago gigantea* Ait. *J Med Plants Res* **5**, 6770–6779.
15. Rajivgandhi GN, Chackaravarthi G, Ramachandran G, Manoharan N, Ragunathan R, Siddiqi MZ, Alharbi NS, Khaled JM, et al (2022) Synthesis of silver nanoparticle (AgNPs) using phytochemical rich medicinal plant *Lonicera japonica* for improve the cytotoxicity effect in cancer cells. *J King Saud Uni Sci* **34**, 101798.
16. Raunmoon S, Sachak S, Thong-in W, Sonkhayan B, Nasomjai P, Khamai P, Thim-uam A, Khwanchai P, et al (2024) Cotton tree (*Bombax ceiba* L.) flower stamen extract: Turning a food ingredient into a reducing agent for the green synthesis of silver nanoparticles. *ScienceAsia* **50**, 2024030.
17. Hussain A, Alajmi ME, Khan MA, Pervez SA, Ahmed F, Amir S, Husain FM, Khan MS, et al (2019) Biosynthesized silver nanoparticle (AgNP) from *Pandanus odorifer* leaf extract exhibits anti-metastasis and anti-biofilm potentials. *Front Microbiol* **10**, 8.
18. González-Fernández S, Lozano-Iturbe V, García B, Andrés LJ, Menéndez MF, Rodríguez D, Vazquez F, Martín C, et al (2020) Antibacterial effect of silver nanorings. *BMC Microbiol* **20**, 172.
19. Fernandes M, González-Ballesteros N, Da Costa A, Andrés LJ, Menéndez MF, Rodríguez D, Vazquez F, et al (2023) Antimicrobial and anti-biofilm activity of silver nanoparticles biosynthesized with *Cystoseira* algae extracts. *J Biol Inorg Chem* **28**, 439–450.
20. Lan LF, Murray TS, Kazmierczak BI, He C (2010) *Pseudomonas aeruginosa* OspR is an oxidative stress sensing regulator that affects pigment production, antibiotic resistance and dissemination during infection. *Mol Microbiol* **75**, 76–91.
21. Muthuchamy M, Govindan R, Shine K, Veeramani T, Alharbi NS, Muneeswaran T, Khaled JM, Jun-Li W, et al (2019) Anti-biofilm investigation of graphene/chitosan nanocomposites against biofilm producing *P. aeruginosa* and *K. pneumoniae*. *Carbohydr Polym* **230**, 115646.
22. Li F, Deng LJ, Chen WW, Thangasamy V, Alharbi NS, Thillaichidambaram M, Khaled JM, et al (2021) Inhibitory effect of catechin against *Xanthomonas campestris*. *J Yunnan Agric Univ (Nat Sci)* **36**, 215–222.
23. Wu C, Zhou X, Wei J (2015) Localized surface plasmon resonance of silver nanotriangles synthesized by a versatile solution reaction. *Nanoscale Res Lett* **10**, 354.
24. Agnihotri S, Mukherji S, Mukherji S (2014) Size-controlled silver nanoparticles synthesized over the range 5–100 nm using the same protocol and their antibacterial efficacy. *RSC Adv* **4**, 3974–3983.
25. Pečenka J, Bytešnicková Z, Kiss T, Peňázová E, Baránek M, Eichmeier A, Tekielska D, et al (2021) Silver nanoparticles eliminate *Xanthomonas campestris* pv. *campestris* in cabbage seeds more efficiently than hot water treatment. *Mater Today Commun* **27**, 102284.
26. Sreelatha S, Kumar N, Yin TS, Rajani S (2021) Evaluating the antibacterial activity and mode of action of thymol-loaded chitosan nanoparticles against plant bacterial pathogen *Xanthomonas campestris* pv. *campestris*. *Front Microbiol* **12**, 792737.
27. Ma C, Liu B, Du L, Liu W, Zhu Y, Chen T, Wang Z, et al (2024) Green preparation and antibacterial activity evaluation of AgNPs-*Blumea balsamifera* oil nanoemulsion. *Molecules* **29**, 2009.
28. Rajivgandhi G, Ramachandran G, Chackaravarthi G, Chelliah CK, Maruthupandy M, Quero F, Al-Mekhlafi FA, et al (2022) Preparation of antibacterial Zn and Ni substituted cobalt ferrite nanoparticles for efficient biofilm eradication. *Anal Biochem* **653**, 114787.
29. Rajivgandhi G, Chackaravarthi G, Ramachandran G, Chelliah CK, Muthuchamy M, Quero F, Mothana RA, et al (2022) Effective removal of biofilm formation in *Acinetobacter baumannii* using chitosan nanoparticles loaded plant essential oils. *J King Saud Univ Sci* **34**, 101845.
30. Mishra S, Yang X, Ray S, Fraceto LF, Singh HB (2020) Antibacterial and biofilm inhibition activity of biofabricated silver nanoparticles against *Xanthomonas oryzae* pv. *oryzae* causing blight disease of rice instigates disease suppression. *World J Microbiol Biotechnol* **36**, 55.
31. Lin Y, Liao YY, Huang RX, Li AZ, An SQ, Tang JL, Tang DJ (2021) Extracellular amylase is required for full virulence and regulated by the global posttranscriptional regulator RsmA in *Xanthomonas campestris* Pathovar *campestris*. *Phytopathology* **111**, 1104–1113.
32. Zhao R, Li D, Wang X, Li Z, Yu X, Shentu X (2022) Synergistic and additive interactions of Zhongshengmycin to the chemical insecticide pymetrozine for controlling *Nilaparvata lugens* (Hemiptera: Delphacidae). *Front Physiol* **13**, 875610.
33. Guan Y, Shen P, Lin M, Ye X (2022) Exogenous alanine reverses the bacterial resistance to Zhongshengmycin with the promotion of the P cycle in *Xanthomonas oryzae*. *Antibiotics (Basel)* **11**, 245.
34. Rooj B, Dutta A, Islam S, Mandal U (2018) Green synthesized carbon quantum dots from *Polianthes tuberosa* L. petals for copper (II) and iron (II) detection. *J Fluoresc* **28**, 1261–1267.

Appendix A. Supplementary data

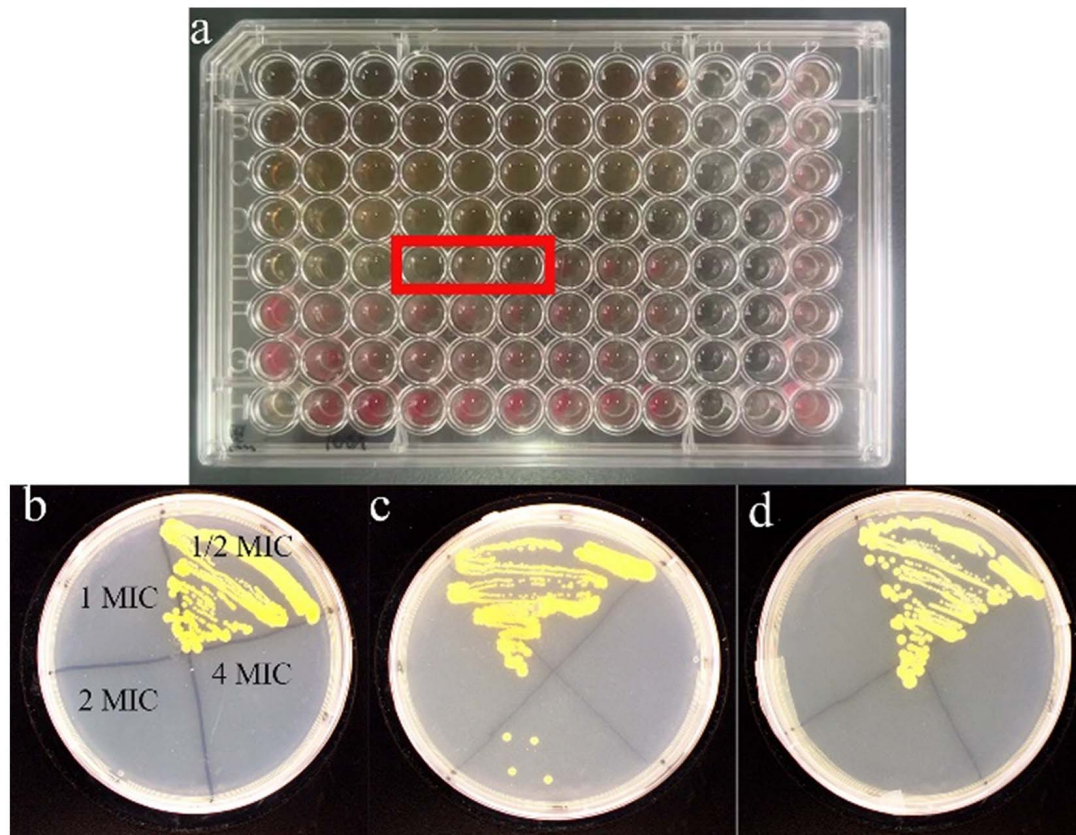


Fig. S1 MIC and MBC determination of AgNPs against *X. compestris*, var. *compestris*. To obtain more accurate MIC values, 3 different starting concentrations of AgNP solutions (200 $\mu\text{g/ml}$ for A1 to A3, 160 $\mu\text{g/ml}$ for A4 to A6, and 120 $\mu\text{g/ml}$ for A7 to A9) (panel a) were used. The first 3 columns (A1–A3) consisted of 3 replicates, denoting a gradual decrease in the concentration of AgNPs in each well from top to bottom, ranging from 200 to 1.5625 $\mu\text{g/ml}$ (H1–H3). Similarly, columns 4–6 and 7–9 exhibited a decreasing trend in the levels of AgNPs, ranging from 160 to 0.078 $\mu\text{g/ml}$ and 120 to 0.056 $\mu\text{g/ml}$, respectively. Columns 10–11 referred to negative control, while column 12 was positive control. Panels b to d were the replicates of MBC test.

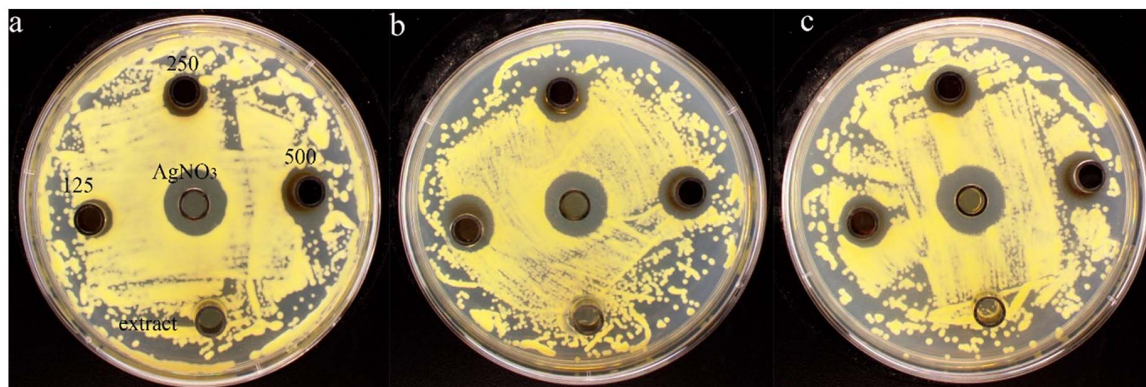


Fig. S2 AgNP bacteriostatic zone of *X. compestris* var. *compestris*.

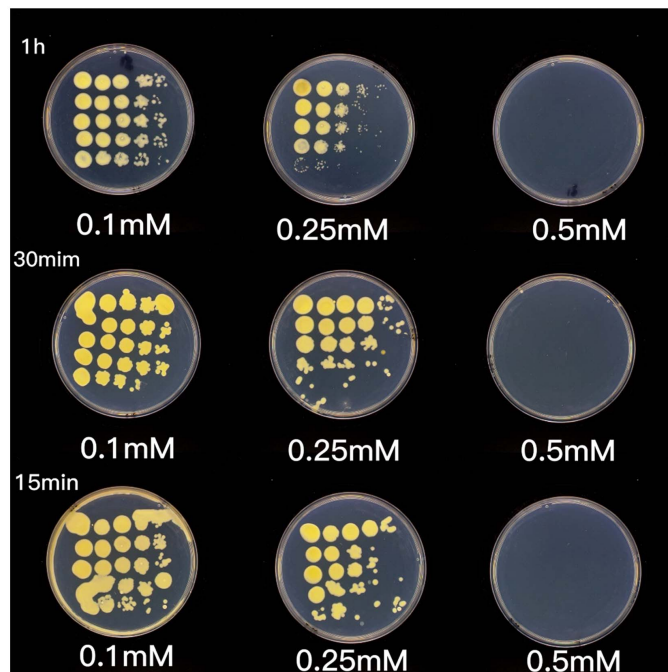


Fig. S3 H_2O_2 tolerance test. On each plate, the AgNP treatments were specified in ascending order, from top to bottom: control, $1/4 \times \text{MIC}$, $1/2 \times \text{MIC}$, $1 \times \text{MIC}$, and $2 \times \text{MIC}$ concentrations. Each row, from left to right, was 5 clones grown in a 10-fold gradient of diluted bacterial solution.

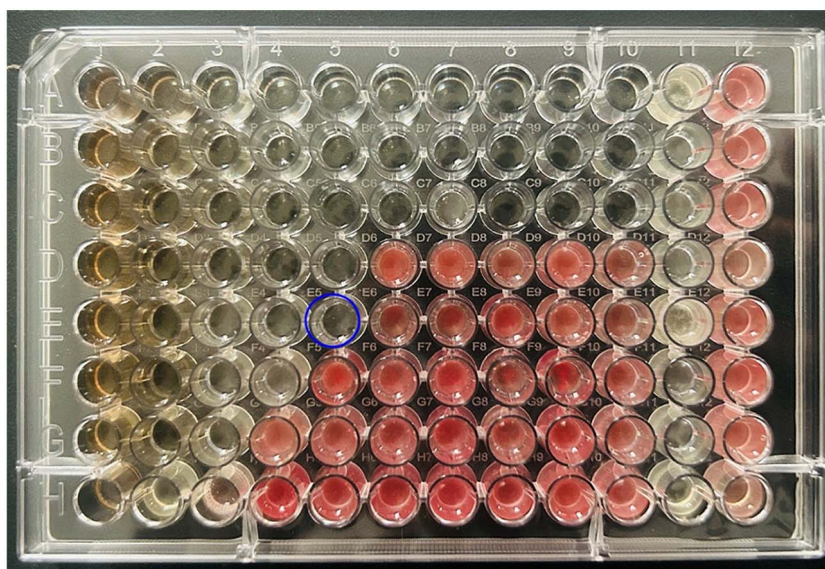


Fig. S4 The synergistic inhibition of AgNPs in combination with Zhongshengmycin on *X. campestris*. The concentration range of zhongshengmycin was 1 to 0.008 $\mu\text{g}/\text{ml}$ with 8 gradients (from row A to row F), while the concentration of AgNPs was set at 20 to 0.04 $\mu\text{g}/\text{ml}$ with 10 gradient sets (from the 1st column to 10th column). The blue circle indicated the well which had no bacterial growth and was used for FIC calculation. The wells in rows 11 and 12 were negative and positive controls, respectively. The controls indicated that the bacterial cells were growing normally, and the operation did not generate the contamination problem.